Monthly Notices of the ROYAL ASTRONOMICAL SOCIETY

MNRAS **529,** 4056–4065 (2024) https://doi.org/10.1093/mnras/stae784
Advance Access publication 2024 March 18

A comprehensive study of orbital evolution of LMC X-4: existence of a second derivative of the orbital period

Chetana Jain [1]★ Rahul Sharma [2]★ and Biswajit Paul[2]

[1]*Hansraj College, University of Delhi, Delhi 110007, India*
[2]*Astronomy & Astrophysics, Raman Research Institute, C.V. Raman Avenue, Bangalore 560080, Karnataka, India*

Accepted 2024 March 13. Received 2024 January 30; in original form 2023 September 30

ABSTRACT

We report here results from pulse arrival time delay analysis of the eclipsing high-mass X-ray binary (HMXB) pulsar LMC X-4 using observations made with the *Rossi X-ray Timing Explorer*, *XMM*–Newton, *NuSTAR* (*Nuclear Spectroscopic Telescope ARray*), and *AstroSat*. Combining the orbital parameters determined from these observations with the historical measurements dating back to 1998, we have extended the $T_{\pi/2}$ epoch history of LMC X-4 by about 4600 binary orbits spanning about 18 yr. We also report mid-eclipse time measurements ($T_{\rm ecl}$) using data obtained from wide-field X-ray monitors of *MAXI*-GSC (Monitor of All-sky X-ray Image – Gas Slit Camera) and *Swift-BAT* (*Burst Alert Telescope*). Combining the new $T_{\pi/2}$ and $T_{\rm ecl}$ estimates with all the previously reported values, we have significantly improved the orbital evolution measurement, which indicates that the orbital period is evolving at a time-scale ($P_{\rm orb}/\dot{P}_{\rm orb}$) of about 0.8 Myr. For the first time in an accreting X-ray pulsar system, we confirm the existence of a second derivative of the orbital period, having an evolution time-scale ($\dot{P}_{\rm orb}/\ddot{P}_{\rm orb}$) of about 55 yr. Detection of a second derivative of the orbital period in LMC X-4 makes its orbital evolution time-scale more uncertain, which may also be true for other HMXBs. Independent solutions for the orbital evolution measurement using the mid-eclipse data and the pulse timing data are consistent with each other, and help us put an upper limit of 0.009 on the eccentricity of the binary system.

Key words: X-rays: binaries – (stars:) pulsars: general – stars: neutron – X-rays – individual: LMC X-4.

1 INTRODUCTION

It has been long realized that most of the bright galactic X-ray sources occur in binary systems (Verbunt 1993; Sana et al. 2012), and binary evolution plays a key role in understanding their stellar evolution (van den Heuvel 1994). Several key astrophysical phenomena, such as the formation of double compact binary (double black holes, black hole–neutron star, and double neutron star systems), followed by the merger of the two stellar components, production of short gamma-ray bursts, and eventually a possible gravitational-wave detection, require a comprehensive understanding of the interaction between the binary components (Belczynski, Kalogera & Bulik 2002). Measurements of the orbital period decay are often used to place limits on the mass transfer and/or rate of mass-loss from the system (Deeter, Boynton & Pravdo 1981). Orbital decay of the famous Hulse–Taylor binary pulsar provided an unprecedented insight into the loss of energy due to gravitational waves, consistent with the general theory of relativity (Taylor & Weisberg 1982).

Being progenitors of double compact objects, the orbital period of X-ray binaries and their evolution have been extensively studied. Important ingredients of such studies include the effect of mass exchange between binary components and mass-loss from the binary system on the orbital parameters. The orbital evolution mechanisms largely include mass transfer (conservative as well as non-conservative) from the companion star to the compact object (van den Heuvel 1994), tidal dissipation in close binaries (Lecar, Wheeler & McKee 1976; Zahn 1977), loss of orbital angular momentum due to stellar winds (Brookshaw & Tavani 1993), gravitational-wave radiation (Verbunt 1993), and magnetic activity associated with the companion star (Wolff et al. 2009; Jain & Paul 2011; Jain, Sharma & Paul 2022).

This work is an accurate and most up-to-date study of the orbital evolution of LMC X-4, which is an eclipsing high-mass X-ray binary (HMXB) system located about 50 kpc away in the Large Magellanic Cloud (LMC; Giacconi et al. 1972). It was discovered in 1972 by the UHURU observatory. This system consists of a 1.25 $M_\odot$ neutron star in an almost circular orbit around a 14th magnitude OB star (Pakull & Olander 1976; Pesch, Sanduleak & Philip 1976; Kelley et al. 1983a; van der Meer et al. 2007). The timing variability of LMC X-4 includes 13.5 s coherent pulsations (Kelley et al. 1983a), ∼26 mHz quasi-periodic oscillations (Rikame et al. 2022; Sharma et al. 2023), about an hour long flaring episodes (Epstein et al. 1977; Skinner et al. 1980; Levine et al. 1991; Beri & Paul 2017), about 5 h long X-ray eclipse (White 1978), an orbital period of ∼1.4 d (Li, Rappaport & Epstein 1978; White 1978) decaying at a rate of about 10^{-6} yr^{-1} (Falanga et al. 2015), and 30.5 d intensity variation due to a precessing tilted accretion disc (Lang et al. 1981; Paul & Kitamoto 2002; Molkov, Lutovinov & Falanga 2015).

★ E-mail: chetanajain11@gmail.com (CJ); rahul1607kumar@gmail.com (RS)

The orbital evolution in eclipsing X-ray binary pulsars is measured using two well-established techniques, namely timing of the X-ray eclipses and the measurement of the orbital epoch using pulse arrival time delays across the orbital phases. The eclipse timing technique is based on the hypothesis that since the binary components revolve around their centre of mass in Keplerian orbits, they are expected to eclipse each other after regular intervals of time. However, if the orbit of the binary is perturbed, then the occurrence of eclipses is delayed (increasing orbit) or is advanced (decreasing orbit) in time. Therefore, in this technique, the mid-eclipse times ($T_{\rm ecl}$) are measured over a sufficiently long time base and time connecting them gives estimates on the orbital period evolution of the system. This method has been used to determine the orbital evolution in several eclipsing X-ray binaries, such as 4U 1822−37 (Jain, Paul & Dutta 2010), AX J1745.6−2901 (Ponti et al. 2017), EXO 0748−676 (Wolff et al. 2009), XTE J1710−281 (Jain & Paul 2011; Jain et al. 2022), MXB 1658−298 (Jain et al. 2017), 4U 1700−37 (Rubin et al. 1996; Falanga et al. 2015; Islam & Paul 2016), etc.

The pulse arrival time technique (Staubert, Klochkov & Wilms 2009) is based on correcting the arrival time of the pulses for the binary motion of the compact object. In this method, the pulse profiles are produced using the already known pulse period, $P_{\rm spin}$ (using χ^2 maximization and epoch folding; Leahy et al. 1983). Assuming t_0 is the reference time of the first pulse, and considering non-zero first derivative of the pulse period, ignoring its higher derivatives, the expected arrival time of the nth pulse (t_n) as a function of the pulse number (n) is given by equation (1),

$$t_n = t_0 + P_{\rm spin} n + \frac{1}{2}\dot{P}_{\rm spin} P_{\rm spin} n^2 + a_x \sin i \cos 2\pi \left(\frac{t - T_{\pi/2}}{P_{\rm orb}}\right). \quad (1)$$

Assuming an almost circular orbit (eccentricity, $e \ll 1$), the fourth term in this equation corresponds to the pulse arrival time delay due to the orbital motion. Here, $a_x \sin i$ is the projected radius of the orbit and $T_{\pi/2}$ is the mean orbital longitude of the neutron star and corresponds to the maximum delay in the pulse arrival time. An important limitation of this method is the fact that this technique requires sufficiently long observations, covering at least a significant part of the binary orbit. This method has been used in X-ray binaries, such as SAX J1808.4−3658 (Jain, Dutta & Paul 2007; Burderi et al. 2009), Her X-1 (Deeter et al. 1991; Staubert et al. 2009), 4U 1538−52 (Baykal, Inam & Beklen 2006; Mukherjee et al. 2006), Cen X-3 (Kelley et al. 1983b; Raichur & Paul 2010a), SAX J1748.9−2021 (Sanna et al. 2016; Sharma et al. 2020), etc.

The first measurements of the pulse arrival time delay in LMC X-4 were reported by Kelley et al. (1983a) using the SAS-3 observations. Later, using the pulse timing analysis, Dennerl (1991) and Levine et al. (1991) established upper limits of $\sim 10^{-6}$ yr^{-1} on the orbital decay. Safi Harb, Ogelman & Dennerl (1996) and Woo et al. (1996) discussed the orbital period decay in LMC X-4 in the context of conservative mass transfer and tidal evolution, superposed by mass-loss from the binary system in the form of stellar winds. Using a long *Rossi X-ray Timing Explorer* (*RXTE*) observation of 1998 October, Levine, Rappaport & Zojcheski (2000) gave the first definite estimate of the decay rate, which was refined by Naik & Paul (2004), Falanga et al. (2015), and Molkov et al. (2015) using data fetched from several X-ray missions.

In this paper, we present an update on the orbital parameters of LMC X-4 using both the methods described above. Historically, the orbital evolution measurements of LMC X-4 have been done using one of these methods or by combining them, but using only a partial set of the available data. For example, Falanga et al. (2015) used only the eclipse data, Levine et al. (2000) and Naik & Paul (2004) used only pulse arrival time data, and Molkov et al. (2015) used a part of available data from both techniques.

The paper is organized in the following way. Section 2 gives a description of the observation and the data reduction procedure. In Section 3, the results from the timing analysis of LMC X-4 are presented. Our findings are discussed in Section 4.

Table 1. Log of X-ray observations of LMC X-4 used in this work.

Observatory	Observation ID	Date YY-MM-DD	Observation span (ks)	Exposure[a] (ks)
RXTE	P10135-01	1996-08-19	132	64
RXTE	P40064-01	1999-12-19	150	60
XMM–Newton	0142800101	2003-09-09	113	55
NuSTAR	10002008001	2012-07-04	62	40
AstroSat	9000000634	2016-08-29	89	31.5

[a] Net exposure after removing flaring, eclipse, and orbital gaps, if any.

2 OBSERVATIONS

The observation details of the narrow field instruments from which data have been used for this work are given in Table 1. For all the data analysed in this work, the source position [RA (J2000) = $05^{\rm h}32^{\rm m}49\overset{\rm s}{.}555$ and Dec. (J2000) = $-66^\circ22'13\overset{''}{.}202$] was adopted from Gaia Collaboration (2021) to convert the photon arrival times to the Solar system barycentre. As described in the previous section, short observations of LMC X-4 have not been used in this work for pulse timing analysis. All the light curves were extracted with a bin time of 0.1 s.

LMC X-4 was observed with *RXTE* (Bradt, Rothschild & Swank 1993) several times between 1996 and 1999, among which Levine et al. (2000) analysed the longest (∼16 d long) observation of 1998 October to obtain a definite measurement of the orbital decay. For this work, we have used data from the observation made with the Proportional Counter Array [PCA; Jahoda et al. (1996) in 1996 August (observation ID 10135-01) and 1999 December (observation ID 40064-01)]. The total span for both of these observations was more than the orbital period of LMC X-4 and for each observation, a useful exposure of ∼60 ks was obtained. We have analysed data collected in the Good Xenon mode having a time resolution of 1 μs. The combined 2–20 keV light curve was extracted using the SEEXTRACT tool of XRONOS sub-package of FTOOLS (Blackburn et al. 1999). The background light curve was extracted from the Standard-2 mode data by using PCABACKEST with a bright source background model (pca_bkgd_cmbrightvle_eMv20051128). Since a different number of PCUs were operational during both the *RXTE* observations therefore we used the CORRECTLC tool to calculate the equivalent count rate for the simultaneous operation of all five PCUs. The time series was barycentre corrected by using FAXBARY.

LMC X-4 was observed six times with *XMM*–Newton (Jansen et al. 2001), out of which Molkov et al. (2015) have reported $T_{\rm ecl}$ measurements from the first two observations. For this work, we have analysed the observation of 2003 September, which had the longest exposure time (∼55 ks) covering about 45 per cent of the binary orbit. *XMM*–Newton carries three focal plane European Photon Imaging Cameras (EPICs) for three X-ray telescopes, EPIC-MOS1, EPIC-MOS2, and EPIC-pn (Strüder et al. 2001; Turner et al. 2001). The raw data files were processed using version 20.0.0 of the *XMM* Science Analysis System (SAS). For the present analysis, we have used 0.5–10 keV data taken with the EPIC-pn detector. The source events were extracted from a circular region of radius 40 arcsec centred on the source position. The background events were extracted from

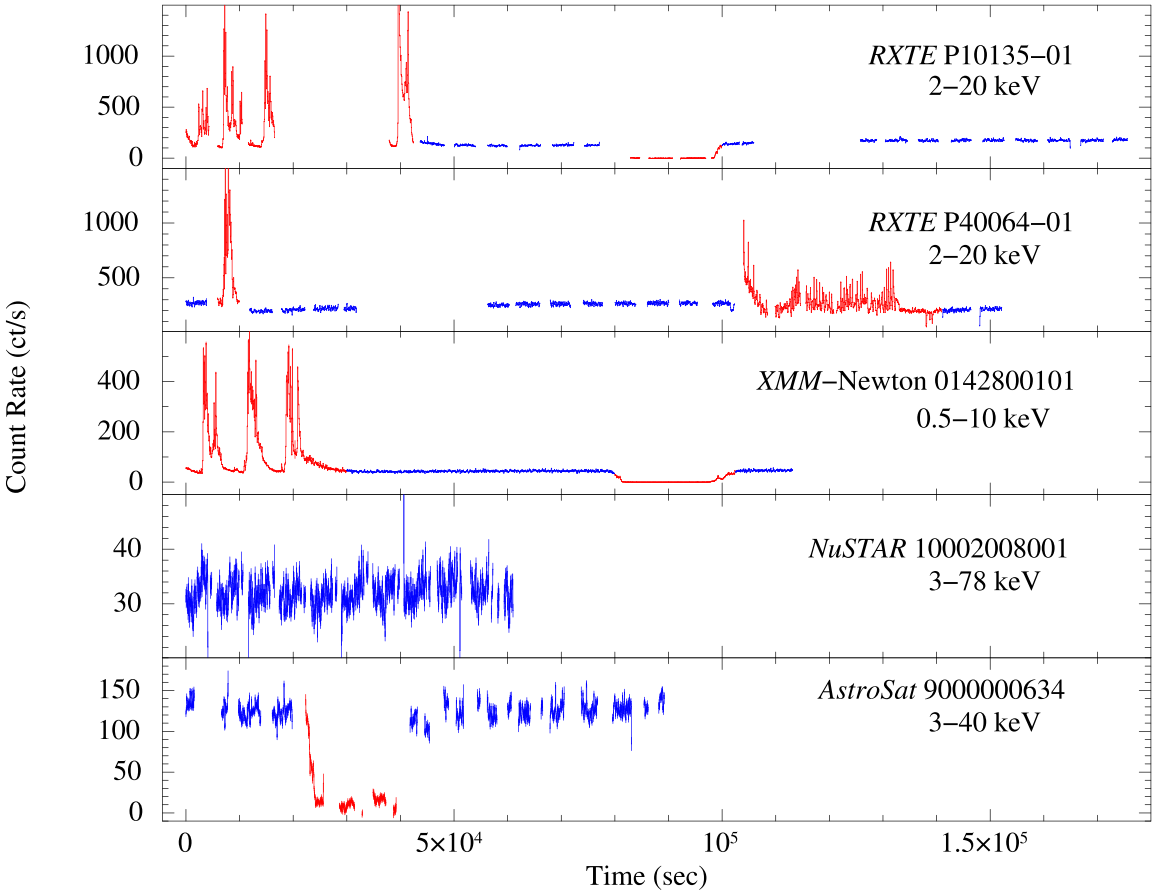

Figure 1. The light curve of LMC X-4 obtained from all the observations listed in Table 1. The respective X-ray mission, observation ID, and energy range are mentioned in each panel. The blue coloured segments were used for the pulse timing measurements. The segments shown in red colour (corresponding to flaring and eclipse phase) were not used.

a similar region centred away from the source location. The event arrival times in the background-subtracted light curve were corrected to the Solar system barycentre using the SAS tool BARYCEN.

The Nuclear Spectroscopic Telescope ARray (*NuSTAR*; Harrison et al. 2013) is a focusing high-energy X-ray telescope that operates in the 3–79 keV energy band. It comprises of two identical focal plane modules [focal plane modules A (FPMA) and B (FPMB)]. For this work, *NuSTAR* observation of 2012 July was used with a duration of 62 ks covering ∼50 per cent of the binary orbit. We have used the standard *NuSTAR* analysis software NUSTARDAS and the latest calibration files (version 20230124) for data reduction and analysis. The clean event files were generated using the NUPIPELINE. Source events were extracted from a circular region of radius 100 arcsec centred at the source position. The background events were extracted from a similar region away from the source location. Barycentre correction was done using BARYCORR. The light curves from both detectors were added for further analysis.

AstroSat is India's first multiwavelength (from optical to hard X-rays) astronomical mission. It was launched by Indian Space Research Organization (ISRO) in 2015 September (Agrawal 2006). Large Area X-ray Proportional Counter (LAXPC; Agrawal et al. 2017) is one of the primary instruments on-board the *AstroSat*. It has a high time resolution of 10 μs and covers a broad X-ray spectral band in 3–80 keV. It consists of three co-aligned proportional counters (LAXPC10, LAXPC20, and LAXPC30), with a total effective area of 6000 cm^{-2} at 15 keV. The *AstroSat* observation of LMC X-4 (observation ID G05_115T01_9000000634) made during 2016 August was analysed for this work. Detailed analysis of this observation has been presented in Sharma et al. (2023). For the current analysis, we used data from LAXPC10 and LAXPC20. LAXPC30 was not used due to gain variability with the instruments (Agrawal et al. 2017; Antia et al. 2017). During this observation, LMC X-4 was observed for a duration of ∼90 ks, covering about 75 per cent of the binary orbit. The Event Analysis mode data from LAXPC10 and LAXPC20 were processed by using the standard LAXPC software.[1] (LAXPCSOFT: version 3.4.2). The light curves for the source and background from both LAXPC units were extracted from level 1 files by using the tool LAXPCL1 and added using LCMATH.

3 TIMING ANALYSIS

The background-subtracted and barycentre corrected light curves of observations listed in Table 1 were filtered for the flaring and eclipse phases. Fig. 1 shows all these five light curves to highlight the segments used and those that were filtered off for the pulse timing measurements.

3.1 $T_{\pi/2}$ measurements

LMC X-4 has an orbital period of ∼1.4 d and semi-amplitude of the arrival time delay due to orbital motion ($a_x \sin i$) of ∼26.3 lt-s. As a result, the pulse frequency gets modulated by the Doppler effect

[1] http://astrosat-ssc.iucaa.in/?q=laxpcData

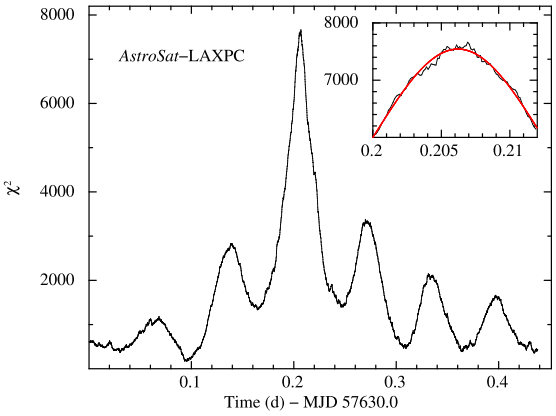

Figure 2. The variation of χ^2 as a function of trial ephemeris for the *AstroSat* observation of LMC X-4. *Inset*: The best-fit Gaussian profile over a narrow range of trial ephemeris.

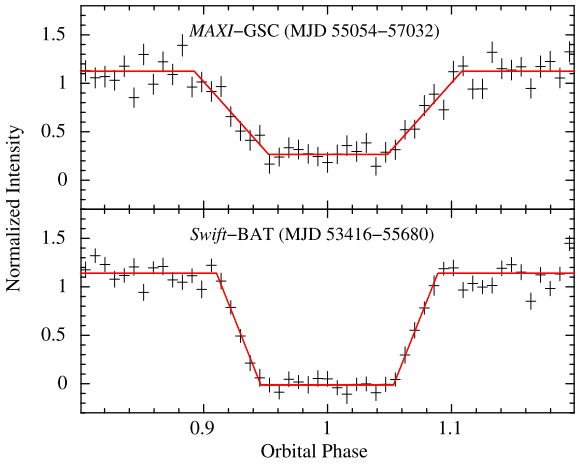

Figure 3. The eclipse profile of the light curve of LMC X-4 obtained from the first segment of the long-term *MAXI*-GSC (top) and *Swift-BAT* (bottom) light curves. The red solid line represents the best-fitting ramp model.

associated with the orbital motion and the pulses are expected to lose coherence within a few thousand seconds. Assuming a nearly circular orbit, we corrected the photon arrival time for the binary motion. The value of $a_x \sin i$ was fixed to the value taken from Levine et al. (2000) and for each observation, $P_{\rm orb}$ was calculated by extrapolating the orbital solution of Molkov et al. (2015).

For all the pointed observations of *RXTE*, *XMM*–Newton, *NuSTAR*, and *AstroSat* tabulated in Table 1, we searched for the correct orbital ephemeris ($T_{\pi/2}$) around the value extrapolated from Molkov et al. (2015). For this, $T_{\pi/2}$ was searched over a wide range of 0.2 d on either side of the extrapolated value in fine steps of $\sim 10^{-4}$ d. We used epoch folding and χ^2 maximization technique (Leahy et al. 1983) for each trial ephemeris. As an example, Fig. 2 shows the variation in χ^2 over the trial range of ephemeris for the *AstroSat* observation. This variation in χ^2 was fit with a Gaussian profile over a narrow range of ± 0.006 d (inset of Fig. 2). We obtained $T_{\pi/2} = 57630.20621(12)$ MJD. The $T_{\pi/2}$ determined from the other observations are listed in Table 2, along with the previously reported measurements. We used the bootstrap method of Boldin, Tsygankov & Lutovinov (2013) to estimate the error in the measurement of $T_{\pi/2}$. Following Sharma et al. (2023), we simulated 1000 light curves and determined the value of $T_{\pi/2}$ in each of them by the epoch folding technique. The standard deviation of $T_{\pi/2}$ measured from all the simulated light curves was taken as 1σ error on $T_{\pi/2}$.

To be doubly sure and to avoid any model dependence, we varied these extrapolated values of $P_{\rm orb}$ by $\pm 2 \times 10^{-5}$ d. We did not find any significant effect of this variation on our measurement of $T_{\pi/2}$.

Table 2. The $T_{\pi/2}$ epoch history of LMC X-4.

Orbit n	$T_{\pi/2}$ (MJD)	Error (d)	Observatory	Reference
−7231	42829.494	0.019	SAS-3	Kelley et al. (1983a)
−4107	47229.3313	0.0004	Ginga	Woo et al. (1996)
−3743	47741.9904	0.0002	Ginga	Levine et al. (1991)
−3163	48558.8598	0.0013	ROSAT	Woo et al. (1996)
−2517	49468.6859	0.0054	ASCA	Paul et al. (2002)
−1978	50227.8069	0.0016	ASCA	Paul et al. (2002)
−1916	50315.12684	0.00008	*RXTE*	This work
−1354	51106.6399	0.0025	Beppo-SAX	Naik & Paul (2004)
−1351	51110.86571	0.00012	*RXTE*[a]	Levine et al. (2000)
−1351	51110.86600	0.00020	*RXTE*[b]	Levine et al. (2000)
−1052	51531.97371	0.00005	*RXTE*	This work
−86	52892.46909	0.00045	*XMM*–Newton	This work
2200	56111.99880	0.00018	*NuSTAR*	This work
3278	57630.20621	0.00012	*AstroSat*	This work

[a] 2–8 keV.
[b] 8–20 keV.

3.2 $T_{\rm ecl}$ measurements

LMC X-4 has been continuously monitored with *Burst Alert Telescope* (*BAT*; Barthelmy et al. 2005; Krimm et al. 2013) on-board the *Swift* observatory (Gehrels et al. 2004) since 2005 and Gas Slit Camera (GSC) on-board the Monitor of All-sky X-ray Image (*MAXI*; Matsuoka et al. 2009; Mihara et al. 2011) since 2009. Therefore, in order to determine a few more mid-eclipse times, we have used the 18 yr long, publicly available 15–50 keV *Swift-BAT* orbital light curve[2] and 14 yr long 2–20 keV *MAXI*-GSC orbital light curve.[3] The photon arrival times were corrected to the solar barycentre reference time by using EARTH2SUN task.

The *Swift-BAT* light curve was divided into three segments spanning about 6 yr, namely MJD 53416–55680, 55680–57943, and 57943–60205. The *MAXI*-GSC light curve was divided into two segments, namely MJD 55054–57032 and 57032–60212. Each of these light curves was folded at local $P_{\rm orb}$ estimated using epoch folding and the mid-eclipse time was estimated using the ramp function. Since all these time segments are relatively long ($\sim$2000 d), it is likely that the orbital period changed during these intervals. Therefore, we also folded the profiles at local $P_{\rm orb}$ and $\dot{P}_{\rm orb}$ obtained from Molkov et al. (2015). There was no significant change in the eclipse time measurement. In fact, use of extrapolated orbital period from Molkov et al. (2015) solution resulted in a similar estimate of the mid-eclipse time, clearly indicating that the period evolution is too slow to have any considerable effect during these time intervals.

Fig. 3 shows the eclipse profile of the first segment of the *MAXI*-GSC and *Swift-BAT* light curve fitted with a ramp function. The mid-eclipse times for these segments were found to be MJD 56042.990(3) and 54547.2978(11), respectively. Table 3 lists the

[2] https://swift.gsfc.nasa.gov/results/transients/LMCX-4/
[3] http://maxi.riken.jp/star_data/J0532-663/J0532-663.html

Table 3. The mid-eclipse (T_{ecl}) epoch history of LMC X-4.

Orbit n	T_{ecl} (MJD)	Error (d)	Observatory	Reference
−7062	43067.51	0.02	SAS-3	Li et al. (1978)
−6957	43215.36	0.02	ESO	Chevalier & Ilovaisky (1977)
−6772	43475.90	0.01	CTIO	Hutchings, Crampton & Cowley (1978)
−5721	44956.15	0.01	ESO	Ilovaisky et al. (1984)
−5227	45651.917	0.015	EXOSAT	Dennerl (1991)
−5224	45656.154	0.008	EXOSAT	Pietsch et al. (1985)
−4662	46447.668	0.011	EXOSAT	Dennerl (1991)
−4638	46481.467	0.003	EXOSAT	Dennerl (1991)
−1916	50315.130	0.015	*RXTE*-PCA	Molkov et al. (2015)
−1614	50740.460	0.015	*RXTE*-PCA	Molkov et al. (2015)
−1611	50744.670	0.015	*RXTE*-PCA	Molkov et al. (2015)
−1349	51113.680	0.015	*RXTE*-PCA	Molkov et al. (2015)
−1090	51478.454	0.008	*RXTE*-ASM	Falanga et al. (2015)
−260	52647.408	0.007	INTEGRAL	Molkov et al. (2015)
−259[a]	52648.804	0.006	INTEGRAL	Molkov et al. (2015)
−86	52892.474	0.015	*XMM*–Newton	Molkov et al. (2015)
0[a]	53013.588	0.004	INTEGRAL	Molkov et al. (2015)
2[a]	53016.411	0.004	INTEGRAL	Molkov et al. (2015)
113	53172.732	0.015	*XMM*–Newton	Molkov et al. (2015)
887	54262.825	0.008	*RXTE*-ASM	Falanga et al. (2015)
1089	54547.2978	0.0011	*Swift-BAT*	This work
1662	55354.284	0.009	INTEGRAL	Molkov et al. (2015)
1663	55355.717	0.018	INTEGRAL	Molkov et al. (2015)
1665	55358.531	0.008	INTEGRAL	Molkov et al. (2015)
1678	55376.841	0.008	INTEGRAL	Molkov et al. (2015)
1679	55378.252	0.008	INTEGRAL	Molkov et al. (2015)
1680	55379.656	0.005	INTEGRAL	Molkov et al. (2015)
1682	55382.463	0.005	INTEGRAL	Molkov et al. (2015)
1684	55385.294	0.007	INTEGRAL	Molkov et al. (2015)
1765	55499.373	0.006	INTEGRAL	Molkov et al. (2015)
1832	55593.729	0.004	INTEGRAL	Molkov et al. (2015)
1833	55595.130	0.005	INTEGRAL	Molkov et al. (2015)
1834	55596.556	0.013	INTEGRAL	Molkov et al. (2015)
1835	55597.938	0.006	INTEGRAL	Molkov et al. (2015)
1941	55747.234	0.004	INTEGRAL	Molkov et al. (2015)
1942	55748.645	0.005	INTEGRAL	Molkov et al. (2015)
1944	55751.446	0.005	INTEGRAL	Molkov et al. (2015)
2077	55938.778	0.009	INTEGRAL	Molkov et al. (2015)
2151	56042.990	0.003	*MAXI*-GSC	This work
2177	56079.594	0.006	INTEGRAL	Molkov et al. (2015)
2179	56082.424	0.005	INTEGRAL	Molkov et al. (2015)
2198	56109.174	0.014	INTEGRAL	Molkov et al. (2015)
2200	56111.993	0.006	INTEGRAL	Molkov et al. (2015)
2205	56119.037	0.008	INTEGRAL	Molkov et al. (2015)
2221	56141.583	0.008	INTEGRAL	Molkov et al. (2015)
2222	56142.985	0.005	INTEGRAL	Molkov et al. (2015)
2328	56292.271	0.006	INTEGRAL	Molkov et al. (2015)
2329	56293.672	0.005	INTEGRAL	Molkov et al. (2015)
2330	56295.084	0.004	INTEGRAL	Molkov et al. (2015)
2438	56447.192	0.007	INTEGRAL	Molkov et al. (2015)
2439	56448.602	0.006	INTEGRAL	Molkov et al. (2015)
2440	56450.014	0.005	INTEGRAL	Molkov et al. (2015)
2442	56452.824	0.008	INTEGRAL	Molkov et al. (2015)
2460	56478.170	0.004	INTEGRAL	Molkov et al. (2015)
2464	56483.794	0.008	INTEGRAL	Molkov et al. (2015)
2696	56810.540	0.001	*Swift-BAT*	This work
3982	58621.689	0.003	*MAXI*-GSC	This work
4303	59073.7605	0.0042	*Swift-BAT*	This work

[a] Also reported by Falanga et al. (2015).

Table 4. Updated orbital parameters of LMC X-4.

Parameter	Falanga et al. (2015)	Molkov et al. (2015)	Updated values: this work[a] Using T_{ecl}	Using $T_{\pi/2}$	Using $T_{\pi/2}+T_{ecl}$ Quadratic	Using $T_{\pi/2}+T_{ecl}$ Cubic
T_0 (MJD)	53013.5910 (8)	$53013.5878^{+0.0018}_{-0.0015}$	53013.5844(14)	53013.5885(3)	53013.58844(14)	53013.5894(2)
P_{orb} (d)	1.4083790 (7)	$1.40837607^{+4.9\times10^{-7}}_{-6.5\times10^{-7}}$	1.40837583(45)	1.40837574(13)	1.40837572(6)	1.40837655(15)
$\dot{P}_{orb}$ (10^{-9} d d^{-1})	-3.86 ± 0.12	-4.66 ± 0.26	-4.60 ± 0.19	-4.97 ± 0.08	-4.97 ± 0.04	-5.13 ± 0.04
$\dot{P}_{orb}/P_{orb}$ (10^{-6} yr^{-1})	-1.00 (5)	-1.21(7)	-1.19(5)	-1.29(2)	-1.287(10)	-1.33(1)
$\tau_{P_{orb}}$ (10^6 yr)[b]	–	–	0.84	0.77	0.78	0.75
$\ddot{P}_{orb}$ (10^{-13} d d^{-2})	–	–	–	–	–	-2.5(4)
$\ddot{P}_{orb}/\dot{P}_{orb}$ (yr^{-1})	–	–	–	–	–	0.018(3)
$\tau_{\dot{P}_{orb}}$ (yr)[c]	–	–	–	–	–	55

[a] Error in T_0, P_{orb}, and $\dot{P}_{orb}$ have been artificially increased such that respective $\chi^2_{red} \sim 1$.
[b] $\tau_{P_{orb}} = P_{orb}/\dot{P}_{orb}$ is evolution time-scale of orbital period.
[c] $\tau_{\dot{P}_{orb}} = \dot{P}_{orb}/\ddot{P}_{orb}$ is evolution time-scale of orbital period derivative.

previously reported measurements of the mid-eclipse epoch (T_{ecl}) of LMC X-4 along with our estimates from *Swift-BAT* and *MAXI*-GSC.

3.3 Orbital evolution

In order to determine the orbital evolution in LMC X-4, we referred to a constant orbital period $P_0 = 1.40837607$ d at a reference epoch $T_0 = 53013.5878$ MJD (Molkov et al. 2015). Using these numbers, we calculated the orbital cycle (n) for every measurement listed in Tables 2 and 3.

Initially, the orbital epochs were fit with a linear + quadratic (LQ) model to all the 58 measurements of T_{ecl} and 14 measurements of $T_{\pi/2}$, using the relation

$$T_n = \Delta T_0 + \Delta P_{orb} n + \frac{1}{2}\dot{P}_{orb} P_{orb} n^2 + \frac{1}{6}\ddot{P}_{orb} P_{orb}^2 n^3. \quad (2)$$

The first two terms in this equation correspond to the case of a constant orbital period. The third term describes the quadratic nature of the orbital decay in LMC X-4. The best-fitting parameters are given in Table 4 (columns 4 and 5). The best-fitting LQ model had reduced χ^2 of 1.9 (in T_{ecl} measurements) and 28 (in $T_{\pi/2}$ measurements). To be more conservative and to account for much larger than 1 reduced χ^2, we scaled the errors associated with T_0, P_{orb}, and $\dot{P}_{orb}$ by respective factor of $\sqrt{\chi^2_{red}}$ (Elsner et al. 1980; van der Klis & Bonnet-Bidaud 1989; Iaria et al. 2015). Hereafter, this scaling of errors in T_0, P_{orb}, and $\dot{P}_{orb}$ has been done for all the models.

We also fitted the LQ model to the combined 72 measurements of T_{ecl} and $T_{\pi/2}$. The best-fitting model had a χ^2 of 443 for 69 degrees of freedom (d.o.f.). Table 4 (column 6) gives the best-fitting parameters of the LQ model applied to these 72 measurements, along with their 1σ errors (after multiplying by $\sqrt{\chi^2_{red}}$, i.e. $\sim$2.5). For these combined measurements, we also fitted the linear + quadratic + cubic (LQC) model (equation 2) to the orbital epochs, where $\ddot{P}_{orb}$ is the second derivative of the orbital period. The best fit had a χ^2 of 296 for 68 d.o.f. The inclusion of the cubic term improved the fit statistics by $\Delta\chi^2 \sim 147$ for one additional d.o.f. with an F-test probability of 1.7×10^{-7} that corresponds to more than 3σ significance. We found the second period derivative to be $2.5(4) \times 10^{-13}$ d d^{-2} and the evolution time-scale of the period derivative ($\ddot{P}_{orb}/\dot{P}_{orb}$) to be 0.018(3) yr^{-1}. Fig. 4 shows the *observed–calculated* (O–C) residual of orbital epochs of LMC X-4 relative to a constant orbital period, for both LQ and LQC models. For completeness, in order to observe the individual contribution of the quadratic and cubic components, to the net χ^2, Fig. 5 shows the residuals (in units of σ) w.r.t. LQ model (upper panel) and the LQC model (lower panel).

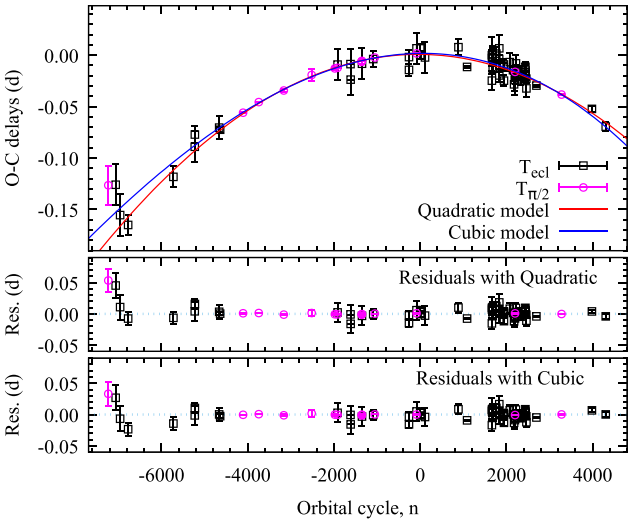

Figure 4. O–C history of LMC X-4 as a function of the orbital cycle, relative to MJD 53013.5878. The data points related to T_{ecl} and $T_{\pi/2}$ have been marked with black and magenta points, respectively, in the top panel. The best-fitting LQ and LQC models are plotted in red and blue colours, respectively. Below two panels show the residuals with LQ and LQC models, respectively.

Among the observations with the narrow field instruments analysed in this work, only the observation from *XMM*–Newton covered a complete X-ray eclipse of LMC X-4. The results from the eclipse timing are already reported in Molkov et al. (2015). However, the errors quoted in Molkov et al. (2015) are as large as 1300 s. This is perhaps due to the post-eclipse dips, which can affect the determination of the eclipse egress profile. The difference between the two measurement techniques and the two orbital evolution models with and without a second derivative of the orbital period is shown in Fig. 6. The vertical dashed lines in this figure correspond to mid-eclipse time measurement obtained from the eclipse timing technique (magenta colour) by Molkov et al. (2015), $T_{\pi/2}$ measured from the pulse timing (reported in Table 2) in red colour and T_n calculated from the best-fitting LQ model (blue colour) and LQC model (green colour). The $T_{\pi/2}$ measurement is closest to the estimates from the LQC model. This inference also supports the fact that the pulse arrival time analysis is much more accurate than the mid-eclipse measurements.

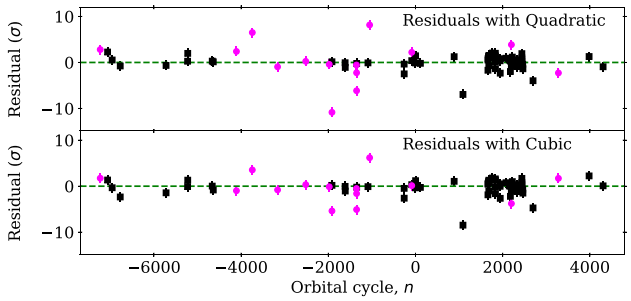

Figure 5. The residual in units of sigma [=(data-model)/error] of the O–C history of LMC X-4 for LQ and LQC models, depicting the individual contribution to the net χ^2. The labelling with black and magenta points is similar to that in Fig. 4.

4 DISCUSSION

In this paper, we have revisited a very well studied HMXB system, LMC X-4, and have made robust estimates of its orbital evolution, by adding new measurements from light curves obtained with the pointed observations made with *RXTE*, *XMM*–Newton, *NuSTAR*, and *AstroSat* and long-term light curves obtained with *Swift-BAT* and *MAXI*-GSC data and thereby spanning the ephemerides history over almost 45 yr. We have determined an orbital period of 1.40837655(15) d at MJD 53013.5894(2), decaying at a rate of $-5.13(4) \times 10^{-9}$ d d^{-1}, with an orbital evolution time-scale of about 0.8 Myr. We have also estimated a second derivative of orbital period $2.5(4) \times 10^{-13}$ d d^{-2}, implying that the orbital decay rate is evolving at a time-scale of just about 55 yr. We discuss these results in the light of the following:

(i) Orbital evolution mechanisms at play in LMC X-4.
(ii) Importance of existence of $\ddot{P}_{\rm orb}$.
(iii) Importance of a non-zero $e \cos \omega$ term.

Orbital evolution has been found to occur in a handful of low-mass X-ray binaries (LMXBs). Among accretion-powered millisecond X-ray pulsars (AMXPs), a rapid orbit expansion has been observed in SWIFT J1749.4−2807 (Sanna et al. 2022), SAX J1808.4−3658 (Jain et al. 2007; Burderi et al. 2009; Illiano et al. 2023), and IGR J17062−6143 (Bult et al. 2021). In few other AMXPs, only the upper limits on the orbital period derivatives are known (Bult et al. 2018; Sanna et al. 2018, 2022), and all are compatible with a rapidly expanding orbit. Among eclipsing LMXBs and/or slowly rotating pulsars, orbital evolution time-scale is known for X2127+119 (Homer & Charles 1998), 4U 1822−37 (Parmar et al. 2000; Jain et al. 2010), AX J1745.6−2901 (Ponti et al. 2017), MXB 1658−298 (Jain et al. 2017), Her X-1 (Deeter et al. 1991; Staubert et al. 2009), 4U 1820−303 (van der Klis et al. 1993; Peuten et al. 2014), EXO 0748−676 (Wolff et al. 2009), and XTE J1710−281 (Jain & Paul 2011; Jain et al. 2022). The orbital evolution in these systems is known to be positive (in X2127+119 and 4U 1822−37), negative (in AX J1745.6−2901, MXB 1658−298, Her X-1, and 4U 1820−303), and has shown sudden changes (again, both positive

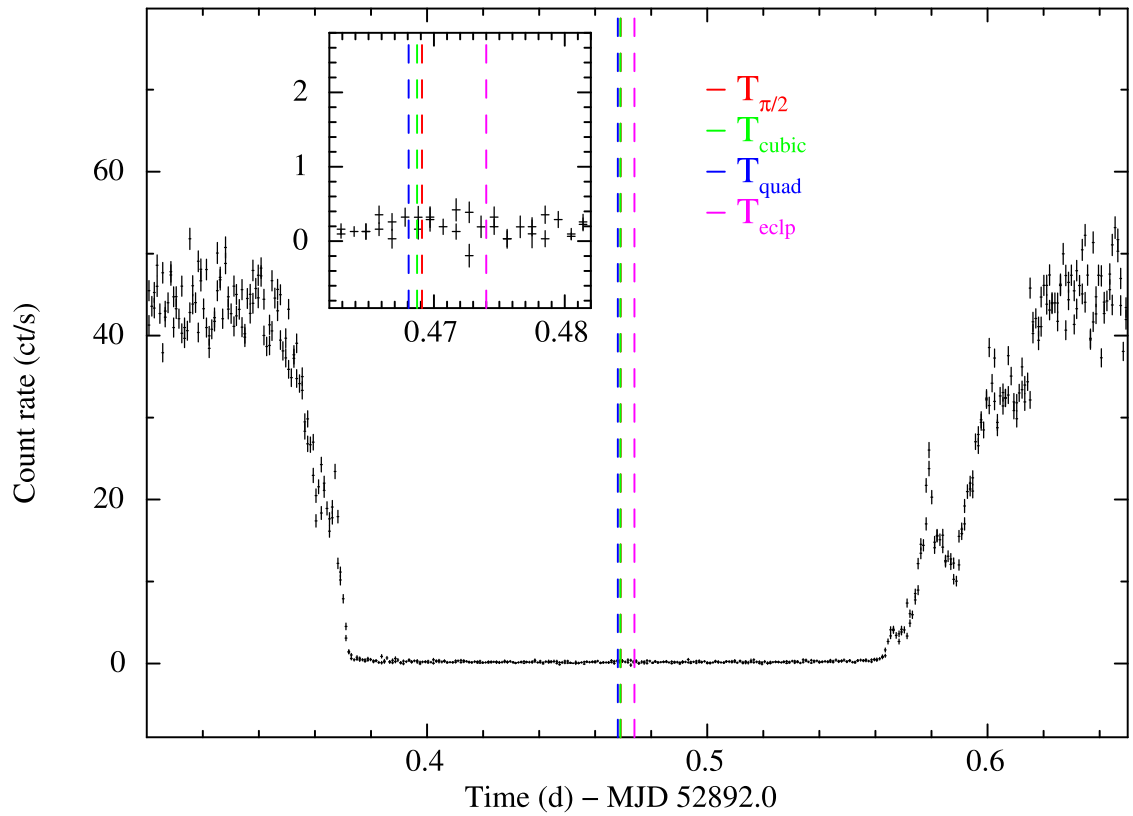

Figure 6. Eclipse profile of the *XMM*–Newton observation (observation ID 0142800101) used in this work. The vertical lines correspond to the expected mid-eclipse time from various techniques. Red: $T_{\pi/2}$, blue: T_n from LQ model, green: T_n from LQC, and Magenta: $T_{\rm ecl}$ from Molkov et al. (2015). The inset shows the zoomed-in section near the centre of the eclipse.

and negative) in period (e.g. EXO 0748−676 and XTE J1710−281), likely due to magnetic cycling in the companion star. The increasing orbital separation in these systems has been attributed to short-lived mass exchange episodes and strong tidal interaction between the binary components. MXB 1658−298 shows an overall orbital period decay influenced by the presence of a massive circumbinary planet. The cause of orbital decay in most LMXBs is inconclusive because the observed time-scale of evolution in these systems (about a million years) is too fast for a conservative Roche lobe mass transfer.

In case of HMXBs, orbital evolution has been found in several systems, such as Cen X-3 (Kelley et al. 1983b; Raichur & Paul 2010a; Klawin et al. 2023), LMC X-4 (Levine et al. 2000; Naik & Paul 2004; Molkov et al. 2015), SMC X-1 (Levine et al. 1993; Wojdowski et al. 1998; Raichur & Paul 2010a), OAO 1657−415 (Jenke et al. 2012), 4U 1700−37 (Rubin et al. 1996; Falanga et al. 2015; Islam & Paul 2016), 4U 1538−52 (Baykal et al. 2006; Mukherjee et al. 2006), GX 301−2 (Doroshenko et al. 2010), and Cyg X-3 (Singh et al. 2002; Bhargava et al. 2017). Orbits of all these binary systems are known to decay, except Cyg X-3. The orbital evolution in Cen X-3, LMC X-4, SMC X-1, and OAO 1657−415 is predominantly due to tidal interactions between the binary components and/or transfer of angular momentum due to strong stellar wind from the binary system to a halo surrounding it. The rate of orbital period decay is much smaller in the case of 4U 1700−37 and 4U 1538−52 than the remaining HMXBs.

Based on the orbital modulation, several authors have studied the changes in the orbital period of Cyg X-3 (van der Klis & Bonnet-Bidaud 1989; Kitamoto et al. 1992, 1995; Singh et al. 2002; Bhargava et al. 2017). Some earlier works based on data before 1990 (van der Klis & Bonnet-Bidaud 1989; Kitamoto et al. 1992) reported a second derivative of the orbital period, but detection was marginal and results were inconclusive. The detection significance of $\ddot{P}_{\rm orb}$ crucially depended on the intrinsic scatter in the data. The inclusion of more data (up to 1993) gave a smaller value $\ddot{P}_{\rm orb}$ (Kitamoto et al. 1995). It was even smaller from data up to 2001 (Singh et al. 2002). The cubic fit to the O–C curve was only marginally better than quadratic fit. The latest works by Bhargava et al. (2017) over 45 yr of time base are biased towards a secular variation in the orbital period without any requirement of a second derivative. They have, however, hinted towards short-term local period variations linked with jet emission.

Assuming a conservative mass transfer in LMC X-4, where the neutron star accretes all the matter lost by its companion, the rate of change of the orbital period is given by (van den Heuvel & de Loore 1973)

$$\dot{P}_{\rm orb}/P_{\rm orb} = 3\frac{(M_{\rm c}-M_{\rm NS})}{M_{\rm c}M_{\rm NS}}\dot{M}_{\rm c}. \tag{3}$$

This gives $\dot{M}_{\rm c} \sim -7.6 \times 10^{-7}\,{\rm M}_{\odot}\,{\rm yr}^{-1}$, assuming orbital decay rate of $\dot{P}_{\rm orb}/P_{\rm orb} = -1.31 \times 10^{-6}$ yr^{-1}, neutron star mass of $M_{\rm NS} = 1.57\,{\rm M}_{\odot}$, and a companion mass of $M_{\rm NS} = 18\,{\rm M}_{\odot}$ (Falanga et al. 2015). This estimate is nearly three times more than the theoretical mass-loss estimate of $\sim -2.4 \times 10^{-7}\,{\rm M}_{\odot}\,{\rm yr}^{-1}$ (Falanga et al. 2015), and it exceeds the Eddington mass accretion limit by a large factor. Clearly, other mass-loss mechanisms are at work in addition to conservative mass transfer and tidal decay.

Assuming a non-conservative mass transfer, where only a fraction of the ejected matter is accreted by the neutron star, following van den Heuvel (1994) and Jenke et al. (2012), and referring to orbital parameters of LMC X-4, we have determined a lower limit on the angular momentum transferred through stellar winds from the companion by using

$$-\dot{P}_{\rm orb}/P_{\rm orb} = -(1+3\gamma)\frac{\dot{M}_{\rm c}}{M_{\rm c}+M_{\rm NS}} - 3\frac{\dot{M}_{\rm c}}{M_{\rm c}}, \tag{4}$$

where γ is the ratio of escaping angular momentum per unit mass to the total angular momentum per unit mass and given by

$$\gamma = \frac{(M_{\rm c}+M_{\rm NS})^2}{M_{\rm c}\,M_{\rm NS}}\left(\frac{a_{\rm e}}{a(1-e^2)}\right)^{1/2}, \tag{5}$$

where a is the semimajor axis of the orbit and $a_{\rm e}$ is the radius beyond the L_2 point of the system of escaping material. Assuming $a_{\rm e} > 1.2a$, neutron star mass of $M_{\rm NS} = 1.57\,{\rm M}_{\odot}$, a companion mass of $M_{\rm NS} = 18\,{\rm M}_{\odot}$, and mass-loss rate of $M_{\rm c} \sim -2.4 \times 10^{-7}\,{\rm M}_{\odot}\,{\rm yr}^{-1}$ (Falanga et al. 2015), we get a decay rate of $>-1.4 \times 10^{-6}$ yr^{-1}. This is well consistent with the observed $\dot{P}_{\rm orb}/P_{\rm orb}$ value of -1.3×10^{-6} yr^{-1}.

For most binary systems, one can measure the period derivative and a first-order estimate for the orbital evolution time-scale. However, if the period derivative itself changes over time, then this estimation is inaccurate. We, for the first time, have determined a second derivative of the orbital period, which turns out to be quite short. So the period evolution time-scale that is measured today is perhaps not valid in a few decades. If the same is true for the other HMXBs, then the long-term evolution of HMXBs cannot be estimated from the current measurements of $P_{\rm orb}$ and $\dot{P}_{\rm orb}$. However, LMC X-4 should be observed extensively over the next decade to have a more secure determination of the second period derivative.

For eccentric orbits, $T_{\rm ecl}$ (measured from the eclipse timing technique) generally does not coincide with $T_{\pi/2}$ (determined from the pulse arrival time technique). This time delay, to the first order in eccentricity, is given by

$$T_{\pi/2} = T_{\rm ecl} + \frac{e\,P_{\rm orb}}{\pi}\cos\omega, \tag{6}$$

where ω is the argument of periapsis (Falanga et al. 2015). In case of LMC X-4, the difference in the best-fitting value of T_0 from $T_{\rm ecl}$ and $T_{\pi/2}$ measurements is 0.0041(14) d, which implies a value of $\sim$0.009(3) for $e\cos\omega$.

The tidal interaction between the binary components of HMXBs is known to circularize their orbit. As a result, the systems among these with small orbital periods (of up to 4 d) have very low eccentricity. Updated orbital solution for HMXBs is important because a good estimate of eccentricity of the orbit has a potential to constrain the age of the binary system and also serve as indirect detection of gravitational-wave emission from the system. Likewise, a good estimate of the periastron angle and advancement of the periastron angle with time (e.g. 4U 0115+63; Raichur & Paul 2010b) is a clue to understanding the stellar structure models of these massive binary systems. Our estimate of $e\cos\omega$ in the case of LMC X-4 can serve as an important ingredient in determining these numbers.

ACKNOWLEDGEMENTS

We thank the anonymous referee for insightful comments and suggestions. This research has made use of archival data and software provided by NASA's High Energy Astrophysics Science Archive Research Center (HEASARC), which is a service of the Astrophysics Science Division at NASA/GSFC. This work has made use of data from the *AstroSat* mission of the Indian Space Research Organisation (ISRO), archived at the Indian Space Science Data Centre (ISSDC).

We thank the LAXPC Payload Operation Center (POC) at TIFR, Mumbai for providing necessary software tools. This research has also used data from *Swift-BAT* and *MAXI*-GSC.

DATA AVAILABILITY

Data used in this work can be accessed through the ISSDC at https://astrobrowse.issdc.gov.in/astro_archive/archive/Home.jsp and HEASARC archive at https://heasarc.gsfc.nasa.gov/cgi-bin/W3Browse/w3browse.pl.

REFERENCES

Agrawal P. C., 2006, Adv. Space Res., 38, 2989
Agrawal P. C. et al., 2017, JA&A, 38, 30
Antia H. M. et al., 2017, ApJS, 231, 10
Barthelmy S. D. et al., 2005, Space Sci. Rev., 120, 143
Baykal A., Inam S. Ç., Beklen E., 2006, A&A, 453, 1037
Belczynski K., Kalogera V., Bulik T., 2002, ApJ, 572, 407
Beri A., Paul B., 2017, New Astron., 56, 94
Bhargava Y. et al., 2017, ApJ, 849, 141
Blackburn J. K., Shaw R. A., Payne H. E., Hayes J. J. E., Heasarc, 1999, Astrophysics Source Code Library, record ascl:9912.002
Boldin P. A., Tsygankov S. S., Lutovinov A. A., 2013, Astron. Lett., 39, 375
Bradt H. V., Rothschild R. E., Swank J. H., 1993, A&AS, 97, 355
Brookshaw L., Tavani M., 1993, ApJ, 410, 719
Bult P. et al., 2018, ApJ, 864, 14
Bult P., Strohmayer T. E., Malacaria C., Ng M., Wadiasingh Z., 2021, ApJ, 912, 120
Burderi L., Riggio A., di Salvo T., Papitto A., Menna M. T., D'Aì A., Iaria R., 2009, A&A, 496, L17
Chevalier C., Ilovaisky S. A., 1977, A&A, 59, L9
Deeter J. E., Boynton P. E., Pravdo S. H., 1981, ApJ, 247, 1003
Deeter J. E., Boynton P. E., Miyamoto S., Kitamoto S., Nagase F., Kawai N., 1991, ApJ, 383, 324
Dennerl K., 1991, Thesis, Ludwig-Maximilians Univ. Max-Planck-Inst. für Physik und Astrophysik, Garching, Germany
Doroshenko V., Santangelo A., Suleimanov V., Kreykenbohm I., Staubert R., Ferrigno C., Klochkov D., 2010, A&A, 515, A10
Elsner R. F., Ghosh P., Darbro W., Weisskopf M. C., Sutherland P. G., Grindlay J. E., 1980, ApJ, 239, 335
Epstein A., Delvaille J., Helmken H., Murray S., Schnopper H. W., Doxsey R., Primini F., 1977, ApJ, 216, 103
Falanga M., Bozzo E., Lutovinov A., Bonnet-Bidaud J. M., Fetisova Y., Puls J., 2015, A&A, 577, A130
Gaia Collaboration, et al., 2021, A&A, 649, A1
Gehrels N. et al., 2004, ApJ, 611, 1005
Giacconi R., Murray S., Gursky H., Kellogg E., Schreier E., Tananbaum H., 1972, ApJ, 178, 281
Harrison F. A. et al., 2013, ApJ, 770, 103
Homer L., Charles P. A., 1998, New Astron., 3, 435
Hutchings J. B., Crampton D., Cowley A. P., 1978, ApJ, 225, 548
Iaria R. et al., 2015, A&A, 582, A32
Illiano G. et al., 2023, ApJ, 942, L40
Ilovaisky S. A., Chevalier C., Motch C., Pakull M., van Paradijs J., Lub J., 1984, A&A, 140, 251
Islam N., Paul B., 2016, MNRAS, 461, 816
Jahoda K., Swank J. H., Giles A. B., Stark M. J., Strohmayer T., Zhang W., Morgan E. H., 1996, in Siegmund O. H., Gummin M. A., eds, Proc. SPIE Conf. Ser. Vol. 2808, EUV, X-Ray, and Gamma-Ray Instrumentation for Astronomy VII. SPIE, Bellingham, p. 59
Jain C., Paul B., 2011, MNRAS, 413, 2
Jain C., Dutta A., Paul B., 2007, JA&A, 28, 197
Jain C., Paul B., Dutta A., 2010, MNRAS, 409, 755
Jain C., Paul B., Sharma R., Jaleel A., Dutta A., 2017, MNRAS, 468, L118
Jain C., Sharma R., Paul B., 2022, MNRAS, 517, 2131
Jansen F. et al., 2001, A&A, 365, L1
Jenke P. A., Finger M. H., Wilson-Hodge C. A., Camero-Arranz A., 2012, ApJ, 759, 124
Kelley R. L., Jernigan J. G., Levine A., Petro L. D., Rappaport S., 1983a, ApJ, 264, 568
Kelley R. L., Rappaport S., Clark G. W., Petro L. D., 1983b, ApJ, 268, 790
Kitamoto S., Mizobuchi S., Yamashita K., Nakamura H., 1992, ApJ, 384, 263
Kitamoto S. et al., 1995, PASJ, 47, 233
Klawin M., Doroshenko V., Santangelo A., Ji L., Ducci L., Bu Q., Zhang S.-N., Zhang S., 2023, A&A, 675, A135
Krimm H. A. et al., 2013, ApJS, 209, 14
Lang F. L. et al., 1981, ApJ, 246, L21
Leahy D. A., Darbro W., Elsner R. F., Weisskopf M. C., Sutherland P. G., Kahn S., Grindlay J. E., 1983, ApJ, 266, 160
Lecar M., Wheeler J. C., McKee C. F., 1976, ApJ, 205, 556
Levine A., Rappaport S., Putney A., Corbet R., Nagase F., 1991, ApJ, 381, 101
Levine A., Rappaport S., Deeter J. E., Boynton P. E., Nagase F., 1993, ApJ, 410, 328
Levine A. M., Rappaport S. A., Zojcheski G., 2000, ApJ, 541, 194
Li F., Rappaport S., Epstein A., 1978, Nature, 271, 37
Matsuoka M. et al., 2009, PASJ, 61, 999
Mihara T. et al., 2011, PASJ, 63, S623
Molkov S. V., Lutovinov A. A., Falanga M., 2015, Astron. Lett., 41, 562
Mukherjee U., Raichur H., Paul B., Naik S., Bhatt N., 2006, JA&A, 27, 411
Naik S., Paul B., 2004, ApJ, 600, 351
Pakull M. W., Olander, 1976, IAU Circ., 3017, 3
Parmar A. N., Oosterbroek T., Del Sordo S., Segreto A., Santangelo A., Dal Fiume D., Orlandini M., 2000, A&A, 356, 175
Paul B., Kitamoto S., 2002, JA&A, 23, 33
Paul B., Nagase F., Endo T., Dotani T., Yokogawa J., Nishiuchi M., 2002, ApJ, 579, 411
Pesch P., Sanduleak N., Philip A. G. D., 1976, IAU Circ., 3023, 2
Peuten M., Brockamp M., Küpper A. H. W., Kroupa P., 2014, ApJ, 795, 116
Pietsch W., Pakull M., Voges W., Staubert R., 1985, Space Sci. Rev., 40, 371
Ponti G., De K., Muñoz-Darias T., Stella L., Nandra K., 2017, MNRAS, 464, 840
Raichur H., Paul B., 2010a, MNRAS, 401, 1532
Raichur H., Paul B., 2010b, MNRAS, 406, 2663
Rikame K., Paul B., Pradhan P., Paul K. T., 2022, MNRAS, 512, 4792
Rubin B. C. et al., 1996, ApJ, 459, 259
Safi Harb S., Ogelman H., Dennerl K., 1996, ApJ, 456, L37
Sana H. et al., 2012, Science, 337, 444
Sanna A. et al., 2016, MNRAS, 459, 1340
Sanna A. et al., 2018, A&A, 616, L17
Sanna A. et al., 2022, MNRAS, 514, 4385
Sharma R., Beri A., Sanna A., Dutta A., 2020, MNRAS, 492, 4361
Sharma R., Jain C., Rikame K., Paul B., 2023, MNRAS, 519, 1764
Singh N. S., Naik S., Paul B., Agrawal P. C., Rao A. R., Singh K. Y., 2002, A&A, 392, 161
Skinner G. K. et al., 1980, ApJ, 240, 619
Staubert R., Klochkov D., Wilms J., 2009, A&A, 500, 883
Strüder L. et al., 2001, A&A, 365, L18
Taylor J. H., Weisberg J. M., 1982, ApJ, 253, 908
Turner M. J. L. et al., 2001, A&A, 365, L27
van den Heuvel E. P. J., 1994, in Saas-Fee Advanced Course 22: Interacting Binaries. Springer, Berlin, p. 263
van den Heuvel E. P. J., de Loore C., 1973, Nat. Phys. Sci., 245, 117
van der Klis M., Bonnet-Bidaud J. M., 1989, A&A, 214, 203
van der Klis M. et al., 1993, MNRAS, 260, 686
van der Meer A., Kaper L., van Kerkwijk M. H., Heemskerk M. H. M., van den Heuvel E. P. J., 2007, A&A, 473, 523
Verbunt F., 1993, ARA&A, 31, 93

White N. E., 1978, Nature, 271, 38
Wojdowski P., Clark G. W., Levine A. M., Woo J. W., Zhang S. N., 1998, ApJ, 502, 253
Wolff M. T., Ray P. S., Wood K. S., Hertz P. L., 2009, ApJS, 183, 156
Woo J. W., Clark G. W., Levine A. M., Corbet R. H. D., Nagase F., 1996, ApJ, 467, 811
Zahn J. P., 1977, A&A, 57, 383

This paper has been typeset from a TEX/LATEX file prepared by the author.